The theory of scaled electromagnetism

OPEN ACCESS

The Theory of Scaled Electromagnetism

Keith Davey[a,*], Hamed Sadeghi[b], Rooholamin Darvizeh[a]

[a]School of Engineering, The University of Manchester, Manchester, UK
[b]Faculty of Mechanical Engineering, University of Guilan, Rasht, Iran

Abstract

Scaled experimentation is an important experimental approach but is known to be limited by scale effects, which have the undesirable effect of changing the behaviour of a system with scale. Such behavioural changes with scale can on occasions be so marked to make a scaled experiment almost worthless. Until very recently there has been no universal solution to this problem with most scaled experiments founded on dimensional analysis and modified necessarily with ad-hoc scaling rules.

This paper is concerned with the development and application of a new approach to scaled experimentation called finite similitude for electro-magnetic systems. It is shown how the finite-similitude theory can be applied to electromagnetism and the governing Maxwell equations in their macroscopic form. The ability of the theory to account for scale dependencies is investigated to reveal the benefits of performing two scaled experiments in describing system behaviour.

keywords: scaling; electromagnetism; finite similitude; trial experimentation; scale effects.

*Corresponding author
Email address: keith.davey@manchester.ac.uk (Keith Davey)

1. Introduction

Scaled models of prototypes and processes have a long history with an almost limitless number of applications across many fields of engineering. Models have been created for marine structures, transport systems, military applications, manufacturing systems, infrastructure, ecosystems, bio-systems along with a multitude of specialist mechanical, structural, fluid and electrical systems (see books and recent reviews [1] [2] [3] [4] [5] [6] [7] [8]). Despite being over one century old the state-of-the-art in scaled experimentation remains the application of similitude theory involving the dimensionless representation of physics [9]. Similitude theory is that branch of engineering science concerned with establishing necessary and sufficient conditions of similarity for phenomena [8]. Scaled models and processes can be classified as true, adequate or distorted depending on whether they match all the dimensionless quantities, a dominant subset or only some of the dominant ones, respectively [2]. The reality of complex products and processes is distorted models (i.e., scale effects) and despite these being used in present-day experiments, they have reduced usefulness and provide results that often can be difficult to interpret [8].

The importance of scaled experimentation has possibly received fresh impetus with the approach known as Hardware-In-the-Loop (HIL) simulation, which facilitates the efficient testing of embedded systems. The renewed impetus comes from the current interest in electrification involving hybrid systems (e.g., see references [10][11][12][13]) and the realisation that scaled pieces of kit can form the hardware component enabling realistic simulations to be performed efficiently and cost effectively [14]. As discussed in reference [14] however the fundamental drawback with the use of scaled equipment in a HIL simulation is that scale effects can make behaviours unrealistic and remedial action is invariably required to account for this. The only realistic remedy at the present time is the application of dimensional analysis and the application of ad-hoc scaling rules [15]. Although the advantage of HIL simulation is that scaling rules can be easily incorporated, this aspect invariably adds an element of uncertainly into the investigation being performed.

Scaled experimentation has played and still plays an important role in the investigation of electromechanical systems [16]. The importance of understanding how scaling changes behaviour in micro-electromechanical systems (MEMS) for example is the topic of the book by Baglio et al. [1]. Similarly Liu and Bar-Cohen [17] examined the scaling laws relevant to actuation mechanisms (i.e., electrostatic, magnetic, thermal bimetallic, and piezoelectric) important to MEMS. The most readily observable effect of scaling is scale dependencies associated with geometric measures, with length scaling linearly, area quadratically and volume cubically. The fact that there exists scale dependencies however is not the same as *scale effects*, which are associated with changes in system behaviour with scale. Fundamental to understanding behaviours requires first an understanding of the effects of scaling on the governing laws of nature. The focus in this paper is on the scaling of electromagnetic systems and consequently on the effects of scaling on those laws governing such systems, which are the renown *Maxwell equations*. The theory introduced in the paper builds on ex-

isting work underpinned by Newtonian physics in the areas of impact [18][19][20], powder compaction[21], bio-mechanics[22] and metal forming[23]. The purpose of the work presented here is for the first time to examine electromagnetism and its incorporation into a new scaling theory called *finite similitude*. The work presented is an important step towards the creation of a scaling theory for the analysis of electromechanics, facilitating scaled studies into new designs for hybrid machines including traditional devices such as motors and generators along with micro & nano electromechanical systems.

The scaling of Maxwell equations has of course been considered previously as described by Gustafson in his book chapter [24] and noted there is the very early work of Sinclair [25]. More recently is the work of Pries and Hofmann [26], where the scaling of both thermal and Maxwell equations are considered. All previous studies however can be related directly or indirectly back to dimensional analysis, where the scaling rules explicitly assume that proportional fields are involved, i.e., any scaled model required to satisfy the rules of similitude, must have fields that are proportional (see reference [27] for an up-to-date exposition). This rule is to be broken here by abandoning dimensionless representations and turning instead to the metaphysical concept of *space scaling*. The idea has great generality as it can in principle be applied to any physics, where the system of interest is imagined to be scaled by the contraction of space itself. Although practically impossible to achieve, what is possible is the interrogation of the effects such a process has on the governing physics and contrasting these with those equations that describe the scaled experiment.

Finite similitude were first introduced by Davey et al. in reference [23] and has recently been extended to the areas of impact [28], fracture [29] and earthquake [30] mechanics. In order for Maxwell equations to be formalised correctly, coordinate systems pertaining to two inertial frames need to be identified. One frame resides in the physical space, where a full-scale test is to be performed and the other in the trial space, where the scaled experiment is to be run. The theory starts with the metaphysical concept of space scaling, which can be defined by forming a differential relationship between the coordinate points in the physical space $\mathbf{x}_{ps}$ and those in the trial space $\mathbf{x}_{ts}$, i.e, $d\mathbf{x}_{ts} = \beta d\mathbf{x}_{ps}$, where β quantifies the extent of the scaling involved with $\beta < 1$ for contraction, $\beta = 1$ indicating no scaling, and $\beta > 1$ for expansion. In addition, with a focus on Newton physics, a differential relationship between absolute time is assumed to apply, i.e., $dt_{ts} = g dt_{ps}$ where g is a positive function of β. The focus on space naturally gives rise to control volumes, since these are nothing more than moving/deforming regions of space. Although stationary control-volume descriptions are common to electromagnetic theory, moving distorting ones are not so prevalent (the authors could find no reference to them), so some reformulation of the Maxwell equations is required. To achieve this the macroscopic Maxwell equations are introduced in Sec. 2 along with a generic form of transport equation. Electromagnetism in transport form is introduced followed by the important step of projecting trial-space transport equations onto the physical space. This particular mathematical process has the effect of exposing all scale dependencies in electromagnetism and is critical to the whole approach. Attention is returned to

finite similitude in Sec. 3, where investigated is an approach to reveal the hidden scale dependencies, which is achieved by defining a new form of similarity called *first-order finite similitude*. This takes the form of a second-order differential equation, which can be readily integrated to reveal field identities. The theory is applied to relatively simple problems in Sec. 4, which includes a generator, a moving rod in a uniform magnetic field and a resistor-inductor-capacitor (RLC) circuit. The analysis of these systems is restricted to analytical studies and a single scaled experiment to illustrate how the finite similitude theory is applied but additionally to contrast with dimensional analysis. A slightly more involved system is also examined in this section involving the commercial finite element software Abaqus applied to a time-harmonic problem concerned with induced Eddy currents. The problem examines the benefit of first-order finite similitude and two scaled experiments in reducing mismatch between scaled and full-scale responses. The paper ends with a list of conclusions.

2. A transport approach to the Maxwell equations

Maxwell's macroscopic equations need little introduction and are of the form:

$$\nabla \cdot \mathbf{D} = \rho^f \tag{1a}$$

$$\nabla \cdot \mathbf{B} = 0 \tag{1b}$$

$$\nabla \times \mathbf{E} = -\frac{\partial \mathbf{B}}{\partial t} \tag{1c}$$

$$\nabla \times \mathbf{H} = \mathbf{J}^f + \frac{\partial \mathbf{D}}{\partial t} \tag{1d}$$

where for stationary linear materials the electric displacement field $\mathbf{D} = \epsilon \mathbf{E}$ and the magnetising field $\mathbf{H} = \mu^{-1}\mathbf{B}$, with permittivity $\epsilon = \epsilon_0(1 + \chi_e)$ and permeability $\mu = \mu_0(1 + \chi_m)$, and where χ_e and χ_m are electric and magnetic susceptibility, respectively; additionally, $\mathbf{E}$, $\mathbf{B}$ are the electric and magnetic fields, ϵ_0, μ_0 are the electric and magnetic constants (also historically referred to as the permittivity and permeability of free space), ρ^f and $\mathbf{J}^f$ are the charge and current densities for free particles, and the operators $\nabla \cdot$, $\nabla \times$ signify divergence and curl. For a medium moving with velocity $\mathbf{v}$, Eqs. (1) still apply, but the constitutive rules $\mathbf{D} = \epsilon \mathbf{E}$ and $\mathbf{H} = \mu^{-1}\mathbf{B}$ transform into the low velocity approximations $\mathbf{D} = \epsilon \mathbf{E}^*$ and $\mathbf{H}^* = \mu^{-1}\mathbf{B}$, where $\mathbf{E}^* = \mathbf{E} + \mathbf{v} \times \mathbf{B}$ and $\mathbf{H}^* = \mathbf{H} - \mathbf{v} \times \mathbf{D}$ (see reference [31] for greater details).

The relationships $\mathbf{D} = \epsilon \mathbf{E}$ and $\mathbf{H} = \mu^{-1}\mathbf{B}$ can be considered as linear constitutive laws since they provide a link between the applied fields $\mathbf{E}$ and $\mathbf{B}$ and the material response. Being constitutive more complex non-linear forms exist, which are often necessary to capture the complex behaviours of real materials [26]. Observe that Eqs. (1) are in a form that can be readily integrated over a fixed control volume Ω with the application of standard integration theorems to arrive at

$$\int_\Gamma \mathbf{D} \cdot \mathbf{n} dS = \int_\Omega \rho^f dV = Q^f \tag{2a}$$

4

$$\int_\Gamma \mathbf{B} \cdot \mathbf{n} d\Gamma = 0 \tag{2b}$$

$$\oint_C \mathbf{E} \cdot \mathbf{d\ell} = -\frac{\partial}{\partial t} \int_S \mathbf{B} \cdot \mathbf{n} dS \tag{2c}$$

$$\oint_C \mathbf{H} \cdot \mathbf{d\ell} = \int_S \mathbf{J}^f \cdot \mathbf{n} dS + \int_S \frac{\partial \mathbf{D}}{\partial t} \cdot \mathbf{n} dS = I^f + \frac{\partial}{\partial t} \int_S \mathbf{D} \cdot \mathbf{n} dS \tag{2d}$$

where Q^f and I^f is the charge in domain Ω and current passing through surface S with boundary C, respectively arising from free particles.

Although these equations are physically intuitive and useful for a lot of problems their form is not best suited to finite similitude, which is founded on transport relationships for moving/distorting control volumes as discussed in the next subsection.

2.1. Generic Equations

This subsection introduces the generic transport equation pertinent to Maxwell field equations for the trial space along with corresponding partial differential equation. The generic form of the partial differential equation is then contrasted with each of Eqs. (1), and through this procedure representative transport equation are obtained for Maxwell's famous equations. The motion of a control volume in the trial space can be readily described by means of the velocity field $\mathbf{v}_{ts}^*$, which itself is definable in terms of the temporal derivative $\frac{D^*}{D^* t_{ts}} = \frac{\partial}{\partial t_{ts}}\big|_{\chi_{ts}}$, where χ_{ts} is a coordinate point in a reference control volume Ω_{ts}^{*ref}. It is proposed here that for the trial space, the generic-transport equation should take the form,

$$\frac{D^*}{D^* t_{ts}} \int_{\Omega_{ts}^*} \Psi_{ts} dV_{ts}^* - \int_{\Gamma_{ts}^*} \Psi_{ts} \mathbf{v}_{ts}^* \cdot \mathbf{n}_{ts} d\Gamma_{ts}^* = -\int_{\Gamma_{ts}^*} \mathbf{J}_{ts}^\psi \cdot \mathbf{n}_{ts} d\Gamma_{ts}^* + \int_{\Omega_{ts}^*} \mathbf{b}_{ts}^\psi dV_{ts}^* \tag{3}$$

were Ψ_{ts} is a specific vector or scalar density field (i.e., per unit volume), $\mathbf{v}_{ts}^*$ is the control velocity field, $\mathbf{J}_{ts}^\psi$ is a flux density (i.e., transfer rate per unit area), $\mathbf{b}_{ts}^\psi$ is a source density term, $\mathbf{n}_{ts}$ is an outward pointing unit normal on the boundary Γ_{ts}^* for the control volume Ω_{ts}^*.

In order to confirm that this equation is of the correct form it is necessary first to derive the partial differential equation linked to it. Consider then application of standard integral identities:

$$\frac{D^*}{D^* t_{ts}} \int_{\Omega_{ts}^*} \Psi_{ts} dV_{ts} = \int_{\Omega_{ts}^*} \left(\frac{D^* \Psi_{ts}}{D^* t_{ts}} + \Psi_{ts} \nabla \cdot \mathbf{v}_{ts}^* \right) dV_{ts} \tag{4}$$

$$\int_{\Gamma_{ts}^*} \Psi_{ts} \mathbf{v}_{ts}^* \cdot \mathbf{n}_{ts} d\Gamma_{ts} = \int_{\Omega_{ts}^*} \nabla \cdot [\Psi_{ts} \mathbf{v}_{ts}^*] dV_{ts} \tag{5}$$

$$\int_{\Gamma_{ts}^*} \mathbf{J}_{ts}^\psi \cdot \mathbf{n}_{ts} d\Gamma_{ts} = \int_{\Omega_{ts}^*} \nabla \cdot \mathbf{J}_{ts}^\psi dV_{ts} \tag{6}$$

to Eq. (3), to reveal the partial differential equation,

$$\frac{D^* \Psi_{ts}}{D^* t_{ts}} - \mathbf{v}_{ts}^* \cdot \nabla \Psi_{ts} = -\nabla \cdot \mathbf{J}_{ts}^\psi + \mathbf{b}_{ts}^\psi \tag{7}$$

5

which can be returned to a familiar Eulerian form on setting $\mathbf{v}_{ts}^*$ to zero, i.e.,

$$\frac{\partial \Psi_{ts}}{\partial t_{ts}} = -\nabla \cdot \mathbf{J}_{ts}^\psi + \mathbf{b}_{ts}^\psi \tag{8}$$

It is important to appreciate that Eq. (7) is not dependent on the velocity fields $\mathbf{v}_{ts}^*$ since the physics it captures cannot be dependent of the movement of a control volume as that would be meaningless. In fact, Eq. (8) is retuned readily on substitution of the identity $\frac{D^*}{D^* t_{ts}} \equiv \frac{\partial}{\partial t_{ts}} + \mathbf{v}_{ts}^* \cdot \nabla$, confirming its independence on $\mathbf{v}_{ts}^*$.

2.2. Transport Maxwell Equations

The system of Eqs. (1) are required to be transformed into transport-equation form for a moving control volume as this is required for the finite similitude theory. Although the form of Eqs. (1) is well suited to vector calculus, as illustrated in the derivation of Eqs. (2), they are not in the form of Eq. (8). The first step in this transformation process is the representation of these equations in coefficient form, which is achieved with the aid of the Levi-Civita tensor $\hat{\epsilon}^{ijk}$ which takes up the values of one for even permutations of $\{ijk\}$, minus one for odd permutations and zero otherwise. The tensor $\hat{\epsilon}^{ijk}$ provides a convenient tool for the representation of cross product since for example

$$(\nabla \times \mathbf{E})^i = \hat{\epsilon}^{ijk} \partial_j E_k = \partial_j (\hat{\epsilon}^{ijk} E_k) \tag{9}$$

where $\partial_j \equiv \frac{\partial}{\partial x^j}$ and $E_k = \delta_{mk} E^m$, and where δ_{mk} is the Kronecker delta symbol and takes up values of zero or one.

Note that Eq. (9) can be conveniently represented by $\nabla \times \mathbf{E} = \nabla \cdot (\hat{\epsilon} \cdot \mathbf{E})$, which is a more convenient form for representation with the transport equations. Consider then the contrasting of Eq. (7) and Eqs. (1), which provide the following transport equations:

$$0 = -\int_{\Gamma_{ts}^*} \mathbf{D}_{ts} \cdot \mathbf{n}_{ts} d\Gamma_{ts} + \int_{\Omega_{ts}^*} \rho_{ts}^f dV_{ts} \tag{10a}$$

$$0 = \int_{\Gamma_{ts}^*} \mathbf{B}_{ts} \cdot \mathbf{n}_{ts} d\Gamma_{ts} \tag{10b}$$

$$\frac{D^*}{D^* t_{ts}} \int_{\Omega_{ts}^*} \mathbf{B}_{ts} dV_{ts} - \int_{\Gamma_{ts}^*} \mathbf{B}_{ts} \mathbf{v}_{ts}^* \cdot \mathbf{n}_{ts} d\Gamma_{ts} = -\int_{\Gamma_{ts}^*} (\hat{\epsilon} \cdot \mathbf{E}_{ts}) \cdot \mathbf{n}_{ts} d\Gamma_{ts} \tag{10c}$$

$$\frac{D^*}{D^* t_{ts}} \int_{\Omega_{ts}^*} \mathbf{D}_{ts} dV_{ts} - \int_{\Gamma_{ts}^*} \mathbf{D}_{ts} \mathbf{v}_{ts}^* \cdot \mathbf{n}_{ts} d\Gamma_{ts} = \int_{\Gamma_{ts}^*} (\hat{\epsilon} \cdot \mathbf{H}_{ts}) \cdot \mathbf{n}_{ts} d\Gamma_{ts} - \int_{\Omega_{ts}^*} \mathbf{J}_{ts}^f dV_{ts} \tag{10d}$$

Although not independent of the ones consider thus far, an additional transport equation is included here, and that is the conservation equation for charge, since it recognised that ρ^f and $\mathbf{J}^f$ are not necessarily independent. This equation is of the form

$$\frac{D^*}{D^* t_{ts}} \int_{\Omega_{ts}^*} \rho_{ts}^f dV_{ts} + \int_{\Gamma_{ts}^*} (\mathbf{J}^f - \rho_{ts}^f \mathbf{v}_{ts}^*) \cdot \mathbf{n}_{ts} d\Gamma_{ts} = 0 \tag{11}$$

6

and it is noted here for a stationary medium that the current density $\mathbf{J}_{ts}^f$ typically takes the form $\mathbf{J}_{ts}^f = \sigma_{ts}\mathbf{E}_{ts}$ (although not limited to this), where σ_{ts} is a material property termed electrical conductivity (or simply conductivity). For a medium moving with relatively low material velocity $\mathbf{v}_{ts}$ (compared to the speed of light *in vacuo*), Ohm's law $\mathbf{J}_{ts}^f = \sigma_{ts}\mathbf{E}_{ts}$ should be replaced by $\mathbf{J}_{ts}^f - \rho_{ts}^f\mathbf{v}_{ts} = \sigma_{ts}\mathbf{E}_{ts}^*$, where as mentioned above $\mathbf{E}_{ts}^* = \mathbf{E}_{ts} + \mathbf{v}_{ts} \times \mathbf{B}_{ts}$ [31].

Included also for completeness is an equation for volume conservation, which is of the form

$$\frac{D^*}{D^*t_{ts}} \int_{\Omega_{ts}^*} dV_{ts}^* - \int_{\Gamma_{ts}^*} \mathbf{v}_{ts}^* \cdot \mathbf{n}_{ts} d\Gamma_{ts}^* = 0 \tag{12}$$

which is of critical importance in the finite similitude theory.

2.3. Projected electromagnetism

The basic idea discussed in this section is critical to the overall scaling philosophy. The idea is to project scaled versions of Eqs. (10) along with Eq. (11) (and Eq. (12) for completeness) onto the physical space. This is achieved on substitution of $dV_{ts}^* = \beta^3 dV_{ps}^*$, $\mathbf{n}_{ts}d\Gamma_{ts}^* = \beta^2\mathbf{n}_{ps}d\Gamma_{ps}^*$ and $dt_{ts} = gdt_{ps}$ and on multiplication by g and respectively α_0^G, α_0^M, α_0^F, α_0^A, for Maxwell, $\alpha_0^{\rho^f}$ for charge and α_0^1 for volume to provide in slightly different order:

$$\alpha_0^1 T_0^1(\beta) = \frac{D^*}{D^*t_{ps}} \int_{\Omega_{ps}^*} \alpha_0^1 \beta^3 dV_{ps}^* - \int_{\Gamma_{ps}^*} \alpha_0^1 \beta^3 \mathbf{v}_{ps}^* \cdot \mathbf{n}_{ps} d\Gamma_{ps}^* = 0 \tag{13a}$$

$$\alpha_0^{\rho^f} T_0^{\rho^f}(\beta) = \frac{D^*}{D^*t_{ps}} \int_{\Omega_{ps}^*} \alpha_0^{\rho^f} \beta^3 \rho_{ts}^f dV_{ps}^* - \int_{\Gamma_{ps}^*} \alpha_0^{\rho^f} \beta^3 \rho_{ts}^f \mathbf{v}_{ps}^* \cdot \mathbf{n}_{ps} d\Gamma_{ps}^* +$$
$$\int_{\Gamma_{ps}^*} \alpha_0^{\rho^f} g\beta^2 \mathbf{J}_{ts}^f \cdot \mathbf{n}_{ps} d\Gamma_{ps}^* = 0 \tag{13b}$$

$$\alpha_0^G T_0^G(\beta) = -\int_{\Gamma_{ps}^*} \alpha_0^G g\beta^2 \mathbf{D}_{ts} \cdot \mathbf{n}_{ps} d\Gamma_{ps}^* + \int_{\Omega_{ps}^*} \alpha_0^G g\beta^3 \rho_{ts}^f dV_{ps}^* = 0 \tag{13c}$$

$$\alpha_0^M T_0^M(\beta) = \int_{\Gamma_{ps}^*} \alpha_0^M g\beta^2 \mathbf{B}_{ts} \cdot \mathbf{n}_{ps} d\Gamma_{ps}^* = 0 \tag{13d}$$

$$\alpha_0^F T_0^F(\beta) = \frac{D^*}{D^*t_{ps}} \int_{\Omega_{ps}^*} \alpha_0^F \beta^3 \mathbf{B}_{ts} dV_{ps}^* - \int_{\Gamma_{ps}^*} \alpha_0^F \beta^3 \mathbf{B}_{ts}(\mathbf{v}_{ps}^* \cdot \mathbf{n}_{ps}) d\Gamma_{ps}^*$$
$$+ \int_{\Gamma_{ps}^*} \alpha_0^F g\beta^2 (\hat{\epsilon}_{ts} \cdot \mathbf{E}_{ts}) \cdot \mathbf{n}_{ps} d\Gamma_{ps}^* = 0 \tag{13e}$$

$$\alpha_0^A T_0^A(\beta) = \frac{D^*}{D^*t_{ps}} \int_{\Omega_{ps}^*} \alpha_0^A \beta^3 \mathbf{D}_{ts} dV_{ps}^* - \int_{\Gamma_{ps}^*} \alpha_0^A \beta^3 \mathbf{D}_{ts}(\mathbf{v}_{ps}^* \cdot \mathbf{n}_{ps}) d\Gamma_{ps}^*$$
$$+ \int_{\Gamma_{ps}^*} \alpha_0^A g\beta^2 (\hat{\epsilon}_{ts} \cdot \mathbf{H}_{ts}) \cdot \mathbf{n}_{ps} d\Gamma_{ps}^* - \int_{\Omega_{ps}^*} \alpha_0^A g\beta^3 \mathbf{J}_{ts}^f dV_{ps}^* = 0 \tag{13f}$$

where use is made of the velocity field relationship $\mathbf{v}^*_{ts} = g^{-1}\beta\mathbf{v}^*_{ps}$, which can be shown to synchronise control volume movement in the trial and physical spaces [28].

These equations are now in a form where the dependency on β is either explicit or implicit and consequently captures scaling from a different perspective. The explicit terms β^3 and β^2 appearing due to change in geometrical measures are readily recognized but also the fields $\mathbf{D}_{ts}(\beta)$, $\mathbf{H}_{ts}(\beta)$, $\mathbf{E}_{ts}(\beta)$, $\mathbf{B}_{ts}(\beta)$ and so on are seen to be implicitly dependent on β. The objective for scaling in this form is the determination of these hidden dependencies, since once these are known, then scaling is solved. Knowledge about how the fields depend on β means that scaled information from a scaled experiment can be transferred to the full scale. Two routes are available for finding these dependencies with one requiring additional information from the particular physical problem being studied (i.e., boundary conditions, size effects etc.) and the other, a more generic approach, involving the application of similitude rules, which is the focus here.

3. Similitude rules

Similitude rules take the form of scale invariances for Eqs. (13) and effectively impose assumed behaviours on how these equations change with β. Undoubtedly for an arbitrary problem such an imposition will not be correct but nevertheless can in principle form the basis for the design of scaled experiments. In this sense the problem is one of design-of-experiments with the similitude rules providing the means for guiding of the design process. The following definition establishes recursively the similitude rules involving differential identities, where Eqs. (13) are repeatedly scaled and differentiated with respect to β.

Definition 3.1. *The lowest value of k satisfying the identity*

$$T^{\psi}_{k+1} = \frac{d(\alpha^{\psi}_k T^{\psi}_k)}{d\beta} \equiv 0 \tag{14}$$

$\forall \beta > 0$ *is a similitude rule (termed k^{th}-order finite similitude), where $\alpha^{\psi}_k(1) = 1$ and $\alpha^{\psi}_0 T^{\psi}_0 = 0$ are projected transport equations (see Eqs. (13)).*

The similitude rules provided by Definition 3.1 are in the form of differential equations with "initial conditions" set to be at $\beta = \beta_0 = 1$. Note that this means that Eqs. (13) must match the physical-space equations at β_0 and is one reason for the requirement $\alpha^{\psi}_k(1) = 1$. Note in particular for Eqs. (13) that: $\alpha^1_0(1) = \alpha^{\rho^f}_0(1) = \alpha^G_0(1) = \alpha^M_0(1) = \alpha^F_0(1) = \alpha^A_0(1) = 1$ along with $g(1) = 1$ since $dt_{ts}(1) = g(1)dt_{ps} = dt_{ps}$. Additionally the fields (now assumed dependent on β) must satisfy $\rho^f_{ts}(1) = \rho^f_{ps}$, $\mathbf{E}_{ts}(1) = \mathbf{E}_{ps}$, $\mathbf{B}_{ts}(1) = \mathbf{B}_{ps}$, $\mathbf{H}_{ts}(1) = \mathbf{H}_{ps}$ and similarly for other fields. The lowest-order similitude rule (termed *zeroth-order finite similitude*) provided by Definition 3.1 describes the situation where there is no variation of Eqs. (13) with β. The rule coincides with what dimensional analysis provides and in mathematical terms is

$$\frac{d}{d\beta}(\alpha^{\psi}_0 T^{\psi}_0) \equiv 0 \tag{15}$$

8

where ψ for Eqs. (13) can be set to 1, ρ^f, G, M, F or A and the equality sign "$\equiv$" means identical, so that the derivative is identically zero in this identity.

The link to what dimensional analysis gives can be seen on integration Eq. (15) between the limits β_1 and $\beta_0 = 1$ to give the identity $\alpha_0^\psi T_0^\psi(\beta_1) \equiv \alpha_0^\psi T_0^\psi(1) = T_0^\psi(1)$. In essence this equality confirms that the trial-space transport equations do not change with scale. Note the critical role of the scalars α_0^ψ in facilitating a unified approach to all the transport equations, which is similar to making equations dimensionless. Unlike dimensional analysis however the finite similitude approach is not restricted to a single invariance and Definition 3.1 provides a countable infinite number of alternatives. Although Eq. (14) has the advantage of simplicity and infers scale effects (as previously defined) are absent, the reality for most problems is the presence of such effects. Thus in practice $\alpha_0^\psi T_0^\psi$ changes with β and Eq. (14) is not applicable. A solution to this problem is to consider an alternative similitude rule provided by Definition 3.1. The first-order similitude rule is recovered on setting $T_1^\psi = \frac{d}{d\beta}(\alpha_0^\psi T_0^\psi)$ and as outlined in Definition 3.1 apply a new set of scalars α_1^ψ and consider the identity

$$\frac{d}{d\beta}(\alpha_1^\psi T_1^\psi) = \frac{d}{d\beta}(\alpha_1^\psi \frac{d}{d\beta}(\alpha_0^\psi T_0^\psi)) \equiv 0 \tag{16}$$

which if satisfied is termed *first-order finite similitude* and is the focus of this study.

Important features are worth noting about the similitude rules provided by Eq. (14) and one is that lower-order rules are contained in higher-order ones. This feature is an absolute physical necessity as it enables lower-order fields to play an important role in the higher-order theory. In particular, Eq. (15) automatically satisfies Eq. (16) and consequently zeroth-order relationships find an important role in Eq. (16). The order of the derivatives increases with increase in the order of the rule, and it is relative easy to see the zeroth order involves a single derivative, first order involve a second-order derivative and kth order involves a maximum derivative of order k+1. This impacts on the number of scaled experiments required with zeroth order only requiring one, first order requiring two and so on.

3.1. First-order scaling

Since by design, zeroth order is contained in first order, it is necessary and prudent to examine zeroth-order requirements initially to ascertain what relationships should remain zeroth order in form. Eq. (13a) satisfies identity Eq. (15) with $\psi = 1$ on setting uniquely $\alpha_0^1 = \beta^{-3}$, which satisfies $\alpha_0^1(1) = 1$ as required. The identity $\alpha_0^1 = \beta^{-3}$ is in fact a necessary and sufficient solution for Eq. (15) and therefore Eq. (13a) is automatically satisfied in first-order theory. Necessary (although not sufficient) conditions on the scalars can be identified on examination of equations with common fields in Eqs. (13). Note that the scalar field ρ_{ts}^f is common to Eqs. (13b) and (13c) and immediately returns $\alpha_0^{\rho^f}\beta^3 = \alpha_0^G g\beta^3$ or more simply $\alpha_0^G = g^{-1}\alpha_0^{\rho^f}$. Similarly, the displacement field $\mathbf{D}_{ts}$ is common to Eqs. (13c) and (13f), which provides the identity $\alpha_0^G g\beta^2 = \alpha_0^A \beta^3$ or more simply $\alpha_0^A = g\beta^{-1}\alpha_0^G$. Likewise, the magnetic field $\mathbf{B}_{ts}$ is common to

Eqs. (13d) and (13e), which returns $\alpha_0^M g\beta^2 = \alpha_0^F \beta^3$ or more simply $\alpha_0^F = g\beta^{-1}\alpha_0^M$. Finally, the current density $\mathbf{J}_{ts}^f$ is common to Eqs. (13b) and (13f) but does not provide a new distinct identity since it returns $\alpha_0^{\rho^f} g\beta^2 = \alpha_0^A g\beta^3$, which reduces to $\alpha_0^{\rho^f} = \beta\alpha_0^A = g\alpha_0^G$, which is of course $\alpha_0^G = g^{-1}\alpha_0^{\rho^f}$. The identities: $\alpha_0^G = g^{-1}\alpha_0^{\rho^f}$, $\alpha_0^A = g\beta^{-1}\alpha_0^G$ and $\alpha_0^F = g\beta^{-1}\alpha_0^M$ are taken forward to first-order theory. Note that these scalars are set in an attempt to eliminate β from transport Eqs. (13). The scalars α_1^ψ (and higher order scalars) play an identical role to α_0^ψ but for the transport equations $\alpha_1^\psi T_1^\psi = 0$ with $\alpha_1^\psi(1) = 1$, which provides further justification for the similitude rules as defined in Definition 3.1.

Integration of Eq. (16) is required for its solution which can be achieved relatively easily by means of divided differences. Consider first the identities:

$$\alpha_1^\psi T_1^\psi(\beta_2^1) = \alpha_1^\psi \frac{d}{d\beta}(\alpha_0^\psi T_0^\psi)(\beta_2^1) \equiv \alpha_1^\psi(\beta_2^1)\frac{\alpha_0^\psi T_0^\psi(\beta_1) - \alpha_0^\psi T_0^\psi(\beta_2)}{\beta_1 - \beta_2} \tag{17a}$$

$$\alpha_1^\psi T_1^\psi(\beta_1^0) = \alpha_1^\psi \frac{d}{d\beta}(\alpha_0^\psi T_0^\psi)(\beta_1^0) \equiv \alpha_1^\psi(\beta_1^0)\frac{\alpha_0^\psi T_0^\psi(\beta_0) - \alpha_0^\psi T_0^\psi(\beta_1)}{\beta_0 - \beta_1} \tag{17b}$$

with $\beta_2 \leq \beta_2^1 \leq \beta_1$, $\beta_1 \leq \beta_1^0 \leq \beta_0$ (where $\beta_0 = 1$), and note the application of a mean-value theorem to ensure exact identities are returned.

The first-order identity (17) means that $\alpha_1^\psi T_1^\psi(\beta_1^0) \equiv \alpha_1^\psi T_1^\psi(\beta_2^1)$, and consequently substitution of Eqs. (17) gives

$$\alpha_1^\psi(\beta_1^0)\frac{\alpha_0^\psi T_0^\psi(\beta_0) - \alpha_0^\psi T_0^\psi(\beta_1)}{\beta_0 - \beta_1} \equiv \alpha_1^\psi(\beta_2^1)\frac{\alpha_0^\psi T_0^\psi(\beta_1) - \alpha_0^\psi T_0^\psi(\beta_2)}{\beta_1 - \beta_2} \tag{18}$$

which following some manipulation provides

$$\alpha_0^\psi T_0^\psi(\beta_0) \equiv \alpha_0^\psi T_0^\psi(\beta_1) + \left(\frac{\alpha_1^\psi(\beta_2^1)}{\alpha_1^\psi(\beta_1^0)}\right)\left(\frac{\beta_0 - \beta_1}{\beta_1 - \beta_2}\right)(\alpha_0^\psi T_0^\psi(\beta_1) - \alpha_0^\psi T_0^\psi(\beta_2)) \tag{19}$$

or more succinctly

$$\alpha_0^\psi T_0^\psi(\beta_0) \equiv \alpha_0^\psi T_0^\psi(\beta_1) + R_1^\psi(\alpha_0^\psi T_0^\psi(\beta_1) - \alpha_0^\psi T_0^\psi(\beta_2)) \tag{20}$$

where

$$R_1^\psi = \left(\frac{\alpha_1^\psi(\beta_2^1)}{\alpha_1^\psi(\beta_1^0)}\right)\left(\frac{\beta_0 - \beta_1}{\beta_1 - \beta_2}\right) \tag{21}$$

and observe that R_1^ψ is a parameter as a consequence of the indeterminacy of α_1^ψ being an unspecified function of β.

Eq. (20) confirms that it is possible to produce transport equations in the physical space (i.e., $\alpha_0^\psi T_0^\psi(\beta_0) = 0$) from projected trial-space transport equations, raising the possibility that behaviours can be predicted exactly (i.e., $\alpha_0^\psi T_0^\psi(\beta_0 = 1) = T_{ps}^\psi = 0$), where $T_{ps}^\psi = 0$ is a physical space transport equation.

3.2. First-order field relationships

Application of Eq. (20) to transport Eqs. (13) provides relationships of the form

$$\rho_1^f = \rho_{\beta_1}^f + R_1^{\rho^f}(\rho_{\beta_1}^f - \rho_{\beta_2}^f) \tag{22a}$$

$$\mathbf{J}_1^f = \mathbf{J}_{\beta_1}^f + R_1^{\rho^f}(\mathbf{J}_{\beta_1}^f - \mathbf{J}_{\beta_2}^f) \tag{22b}$$

$$\mathbf{D}_1 = \mathbf{D}_{\beta_1} + R_1^{G}(\mathbf{D}_{\beta_1} - \mathbf{D}_{\beta_2}) \tag{22c}$$

$$\rho_1^f = \rho_{\beta_1}^f + R_1^{G}(\rho_{\beta_1}^f - \rho_{\beta_2}^f) \tag{22d}$$

$$\mathbf{B}_1 = \mathbf{B}_{\beta_1} + R_1^{M}(\mathbf{B}_{\beta_1} - \mathbf{B}_{\beta_2}) \tag{22e}$$

$$\mathbf{B}_1 = \mathbf{B}_{\beta_1} + R_1^{F}(\mathbf{B}_{\beta_1} - \mathbf{B}_{\beta_2}) \tag{22f}$$

$$\mathbf{E}_1 = \mathbf{E}_{\beta_1} + R_1^{F}(\mathbf{E}_{\beta_1} - \mathbf{E}_{\beta_2}) \tag{22g}$$

$$\mathbf{D}_1 = \mathbf{D}_{\beta_1} + R_1^{A}(\mathbf{D}_{\beta_1} - \mathbf{D}_{\beta_2}) \tag{22h}$$

$$\mathbf{H}_1 = \mathbf{H}_{\beta_1} + R_1^{A}(\mathbf{H}_{\beta_1} - \mathbf{H}_{\beta_2}) \tag{22i}$$

$$\mathbf{J}_1^f = \mathbf{J}_{\beta_1}^f + R_1^{A}(\mathbf{J}_{\beta_1}^f - \mathbf{J}_{\beta_2}^f) \tag{22j}$$

where $\rho_\beta^f = \alpha_0^{\rho^f}\beta^3\rho_{ps}^f$, $\mathbf{J}_\beta^f = \alpha_0^{\rho^f}g\beta^2\mathbf{J}_{ts}^f$, $\mathbf{D}_\beta = \alpha_0^{G}g\beta^2\mathbf{D}_{ts}$, $\mathbf{B}_\beta = \alpha_0^{M}g\beta^2\mathbf{B}_{ts}$, $\mathbf{E}_\beta = \alpha_0^{F}g\beta^2\mathbf{E}_{ts}$ and $\mathbf{H}_\beta = \alpha_0^{A}g\beta^2\mathbf{H}_{ts}$, and for a consistent field expressions it is required that $R_1^{\rho^f} = R_1^{G} = R_1^{A}$ and $R_1^{M} = R_1^{F}$.

The conditions $R_1^{\rho^f} = R_1^{G} = R_1^{A}$ and $R_1^{M} = R_1^{F}$ are meaningful and are in a sense separating the governing equations into two groups, i.e., Eqs. (13b), (13c), (13f) and Eqs. (13d), (13e), where the latter two equations only involve externally applied fields, i.e., $\mathbf{B}$ and $\mathbf{E}$. It is well appreciated that these equations can be automatically satisfied on application of the gauge identities $\mathbf{E} = -\nabla\phi - \frac{\partial\mathbf{A}}{\partial t}$ and $\mathbf{B} = \nabla\times\mathbf{A}$, where ϕ and $\mathbf{A}$ are known as the scalar and vector potentials, respectively. Equations (13b), (13c) and (13f) on the other hand, being connected by a common R_1 value infer that differences between transport equations and particular fields are proportional. The fields involved are provided by the theory and are ρ_β^f, $\mathbf{J}_\beta^f$, $\mathbf{D}_\beta$, and $\mathbf{H}_\beta$ and separately $\mathbf{B}_\beta$ and $\mathbf{E}_\beta$. The result is a clear departure from zeroth-order finite similitude and dimensional analysis, which only involve proportional fields. Note also that all the differences in the right-hand bracket in Eqs. (22) will be zero if the fields satisfy zeroth-order rules as anticipated by the initial choices made in Definition 3.1.

Relatively simple case studies are analysed in the next section with the aid of the practical zeroth-order and first-order identities listed in Table 1. Note that additional relationships are provided in the table (i.e., charge Q^f, current I^f, magnetic flux Φ, and voltage V) each of which are readily derived from the original identities listed in Eqs. (22). Additionally for a stationary material, the linear material constitutive identities $\mathbf{D}_{ts} = \epsilon_{ts}\mathbf{E}_{ts}$ and $\mathbf{H}_{ts} = \mu_{ts}^{-1}\mathbf{B}_{ts}$ can be substituted respectively into $\mathbf{D}_\beta = \alpha_0^{G}g\beta^2\mathbf{D}_{ts}$ and $\mathbf{H}_\beta = \alpha_0^{A}g\beta^2\mathbf{H}_{ts}$ to reveal $\mathbf{D}_\beta = \epsilon_\beta\mathbf{E}_\beta$ and $\mathbf{H}_\beta = \mu_\beta^{-1}\mathbf{B}_\beta$, where $\alpha_0^{F}\epsilon_\beta = \alpha_0^{G}\epsilon_{ts}$ and $\alpha_0^{M}\mu_\beta^{-1} = \alpha_0^{A}\mu_{ts}^{-1}$.

Table 1: Zeroth and first order relationships.

Zeroth order	First order relationships
$\rho_{ps}^f = \alpha_{01}^{\rho^f}\beta_1^3\rho_{ts1}^f$	$\rho_{ps}^f = \alpha_{01}^{\rho^f}\beta_1^3\rho_{ts1}^f + R_1^{\rho^f}(\alpha_{01}^{\rho^f}\beta_1^3\rho_{ts1}^f - \alpha_{02}^{\rho^f}\beta_2^3\rho_{ts2}^f)$
$Q_{ps}^f = \alpha_{01}^{\rho^f}Q_{ts1}^f$	$Q_{ps}^f = \alpha_{01}^{\rho^f}Q_{ts1}^f + R_1^{\rho^f}(\alpha_{01}^{\rho^f}Q_{ts1}^f - \alpha_{02}^{\rho^f}Q_{ts2}^f)$
$\mathbf{J}_{ps}^f = \alpha_{01}^{\rho^f}g_1\beta_1^2\mathbf{J}_{ts1}^f$	$\mathbf{J}_{ps}^f = \alpha_{01}^{\rho^f}g_1\beta_1^2\mathbf{J}_{ts1}^f + R_1^{\rho^f}(\alpha_{01}^{\rho^f}g_1\beta_1^2\mathbf{J}_{ts1}^f - \alpha_{02}^{\rho^f}g_2\beta_2^2\mathbf{J}_{ts2}^f)$
$I_{ps}^f = \alpha_{01}^{\rho^f}g_1 I_{ts1}^f$	$I_{ps}^f = \alpha_{01}^{\rho^f}g_1 I_{ts1}^f + R_1^{\rho^f}(\alpha_{01}^{\rho^f}g_1 I_{ts1}^f - \alpha_{02}^{\rho^f}g_2 I_{ts2}^f)$
$\mathbf{D}_{ps} = \alpha_{01}^{G}g_1\beta_1^2\mathbf{D}_{ts1}$	$\mathbf{D}_{ps} = \alpha_{01}^{G}g_1\beta_1^2\mathbf{D}_{ts1} + R_1^{G}(\alpha_{01}^{G}g_1\beta_1^2\mathbf{D}_{ts1} - \alpha_{02}^{G}g_2\beta_2^2\mathbf{D}_{ts2})$
$\mathbf{B}_{ps} = \alpha_{01}^{M}g_1\beta_1^2\mathbf{B}_{ts1}$	$\mathbf{B}_{ps} = \alpha_{01}^{M}g_1\beta_1^2\mathbf{B}_{ts1} + R_1^{M}(\alpha_{01}^{M}g_1\beta_1^2\mathbf{B}_{ts1} - \alpha_{02}^{M}g_2\beta_2^2\mathbf{B}_{ts2})$
$\Phi_{ps} = \alpha_{01}^{M}g_1\Phi_{ts1}$	$\Phi_{ps} = \alpha_{01}^{M}g_1\Phi_{ts1} + R_1^{M}(\alpha_{01}^{M}g_1\Phi_{ts1} - \alpha_{02}^{M}g_2\Phi_{ts2})$
$\mathbf{E}_{ps} = \alpha_{01}^{F}g_1\beta_1^2\mathbf{E}_{ts1}$	$\mathbf{E}_{ps} = \alpha_{01}^{F}g_1\beta_1^2\mathbf{E}_{ts1} + R_1^{F}(\alpha_{01}^{F}g_1\beta_1^2\mathbf{E}_{ts1} - \alpha_{02}^{F}g_2\beta_2^2\mathbf{E}_{ts2})$
$V_{ps} = \alpha_{01}^{F}g_1\beta_1 V_{ts1}$	$V_{ps} = \alpha_{01}^{F}g_1\beta_1 V_{ts1} + R_1^{F}(\alpha_{01}^{F}g_1\beta_1 V_{ts1} - \alpha_{02}^{F}g_2\beta_2 V_{ts2})$
$\mathbf{H}_{ps} = \alpha_{01}^{A}g\beta_1^2\mathbf{H}_{ts1}$	$\mathbf{H}_{ps} = \alpha_{01}^{A}g\beta_1^2\mathbf{H}_{ts1} + R_1^{A}(\alpha_{01}^{A}g_1\beta_1^2\mathbf{H}_{ts1} - \alpha_{02}^{A}g_2\beta_2^2\mathbf{H}_{ts2})$

4. Case studies

The efficacy of the new scaling theory for electromagnetism is investigated through the analysis of relatively straightforward case studies, with each study focusing on different aspects of Maxwell equations.

Faraday's law of induction (Eq. (2c)) is examined first, where it is established that the new scaling theory provides good replication of full scale behaviours. This is shown through known analytical solutions and also by contrasting with results obtained from dimensional analysis for pure dimensional scaling (i.e., geometry and temporal changes only). The objective of this study is to showcase zeroth-order finite similitude and highlight its ease of applicability by contrasting it against the more familiar theory of dimensional analysis.

The second case study is the scaling of a simple RLC circuit and is designed to showcase the zeroth-order approach. Replica scaling is considered but scaled behaviour is found to deviate from the full-scale model. It is confirmed however that the circuit can be successfully scaled with replica scaling of the inductor and capacitor, but additionally by ensuring that the circuit resistance remains unchanged.

The third case study is designed to test out the first-order theory by means of a numerical study using the commercial finite element software Abaqus [32]. The problem considered examines Eddy currents and their response to scaling involving Eq. (1d).

4.1. Case Study I: Scaling Faraday's Law of Induction

The impact of scaling on Faraday's law of induction (i.e., Eq. (2c)) is considered and examined by considering simple analytical examples, one involving a circuit with a moving part in a stationary magnetic field, and another consisting of a generator involving a rotating circuit, again in a stationary magnetic

field. Pure dimensional scaling, involving only changes in geometry, is applied initially to ascertain how the behaviour of the scaled models differ from the full scale. This is followed by the application of zeroth-order finite similitude theory, where perfect replication between the scaled and full-scaled models is observed. The equation of interest is Eq. (2c) but it is useful at this stage to define electromotive force (emf) to be $\mathcal{E} = \int_C \mathbf{E} \cdot \mathbf{d}\ell$ and magnetic flux by $\Phi = \int_S \mathbf{B} \cdot \mathbf{n} dS$ and consequently Eq. (2c) simplifies to $\mathcal{E} = -\frac{d\Phi}{dt}$.

4.1.1. Scaling of an adjustable circuit in a magnetic field

Depicted in Fig. 1 is a circuit containing a moving part and consequently the area contained within the circuit is changing but the magnetic field B is assumed fixed and accordingly the magnetic flux Φ in the physical space is given by the relationship $\Phi_{ps} = B_{ps} A_{ps} = B_{ps} \ell_{ps} x_{ps}$, where the lengths ℓ_{ps} and x_{ps} are shown in Fig. 1. It follows therefore that the induced emf $\mathcal{E}_{ps}$ is given by [27]

$$\mathcal{E}_{ps} = -\frac{d\Phi_{ps}}{dt_{ps}} = -\frac{d}{dt_{ps}}(B_{ps}\ell_{ps}x_{ps}) = -B_{ps}\ell_{ps}\frac{dx_{ps}}{dt_{ps}} = -B_{ps}\ell_{ps}v_{ps} \tag{23}$$

and under the assumption that Ohm's law applies the induced current is given by

$$I_{ps} = \left|\frac{\mathcal{E}_{ps}}{R_{ps}}\right| = \frac{B_{ps}\ell_{ps}v_{ps}}{R_{ps}} \tag{24}$$

where R_{ps} is the resistance provided by the circuit.
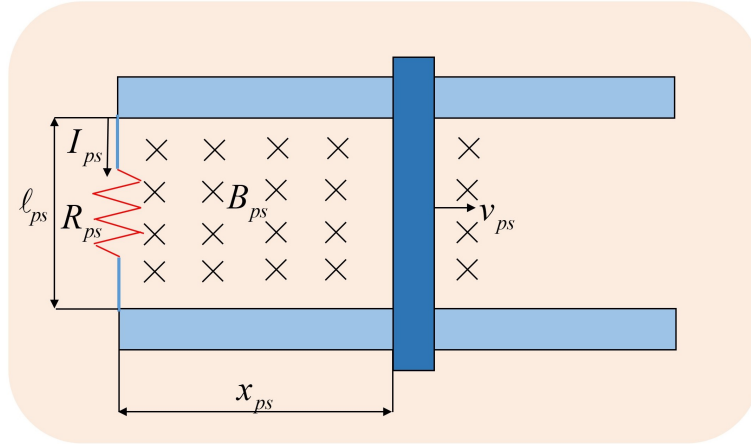

Figure 1: A circuit containing a moving part located in a magnetic field

Pure dimensional scaling

Consider then, geometrically similar small-scale models made out of the same material as the full-scale model. From a dimensional-analysis perspective the problem is relatively straightforward on specification of the Pi group $\Pi = \frac{B\ell v}{IR}$ and the requirement that $\Pi_{ts} = \Pi_{ps}$. Additionally on adoption of the notation applied in finite similitude it can immediately be deduced that length scales as $\ell_{ts} = \beta\ell_{ps}$, area scales as $A_{ts} = \beta^2 A_{ps}$,

and velocity behaves as $v_{ts} = g^{-1}\beta v_{ps}$, which on substitution provides the requirement,

$$\Pi_{ts} = \frac{B_{ts}\ell_{ts}v_{ts}}{I_{ts}R_{ts}} = \frac{\beta^2}{g}\frac{B_{ts}\ell_{ps}v_{ps}}{I_{ts}R_{ts}} = \frac{\beta^3}{g}\frac{B_{ts}\ell_{ps}v_{ps}}{I_{ts}R_{ps}} = \frac{\beta^3}{g}\frac{B_{ts}}{B_{ps}}\frac{I_{ps}}{I_{ts}}\Pi_{ps} \tag{25}$$

where use is made of $R_{ts} = \beta^{-1}R_{ps}$, in view of the relationship for circuit resistance $R = \frac{\rho\ell}{A}$, where ρ is a material property (resistivity), which remains unchanged by assumption.

It transpires therefore that the dimensionless identity $\Pi_{ts} = \Pi_{ps}$ provides a relationship for the induced current to be

$$I_{ts} = \frac{\beta^3}{g}\frac{B_{ts}}{B_{ps}}I_{ps} \tag{26}$$

and under the assumption of a scale invariant magnetic field (i.e., $B_{ts} = B_{ps}$) the induced current is also scale invariant provided $g = \beta^3$, or equivalently rod velocities satisfy $v_{ts} = \beta^{-2}v_{ps}$.

Zeroth-order finite similitude

Finite similitude is not concerned with the forming of dimensionless Pi groups but does provide definitive identities and associated degrees of freedom. The focus on Faraday's law means that the projected equation of particular interest is Eq. (13e) but finite similitude provides solutions for all Maxwell equations. The pertinent zeroth-order field relationships in Table 1 are $\mathbf{J}_{ps}^f = \alpha_0^{\rho^f}g\beta^2\mathbf{J}_{ts}^f$, $\mathbf{B}_{ps} = \alpha_0^M g\beta^2\mathbf{B}_{ts}$, $\mathbf{E}_{ps} = \alpha_0^F g\beta^2\mathbf{E}_{ts}$, and scalar identity $\alpha_0^F = g\beta^{-1}\alpha_0^M$. Note that Ohm's law provides a relationship between electromotive force $\mathcal{E}$ and current I, which in terms of fields (as mentioned above) is equivalent to $\mathbf{J}^f = \sigma\mathbf{E}$, where σ is material conductivity, which is the inverse of resistivity (i.e., $\sigma = \rho^{-1}$). The conditions $\mathbf{B}_{ps} = \mathbf{B}_{ts}$ and $\mathbf{J}_{ps}^f = \beta^2\mathbf{J}_{ts}^f$ (current matching) provides $\alpha_0^M g\beta^2 = 1$ and $\alpha_0^{\rho^f}g\beta^2 = \beta^2$, respectively and consequently $\alpha_0^{\rho^f} = \beta^2\alpha_0^M$. But additionally, Ohm's law for the same material means that $\mathbf{E}_{ps} = \beta^2\mathbf{E}_{ts}$ and consequently $\alpha_0^F g\beta^2 = \beta^2$, which similarly provides $\alpha_0^F = \beta^2\alpha_0^M$, but since $\alpha_0^F = g\beta^{-1}\alpha_0^M$ it follows that $g = \beta^3$. This result is in accordance with dimensional analysis providing the relationship $v_{ts} = \beta^{-2}v_{ps}$ for rod velocities.

4.1.2. Scaling of a generator

Depicted in Fig. 2 is a circuit rotating in an magnetic field for the purposes of current generation, which again obeys Faraday's law, (i.e., Eq. (1c)). The area A_{ps} encircled by the circuit (with unit normal $\mathbf{n}_{ps}$) cuts the magnetic field at an angle θ_{ps}, i.e., $\mathbf{B}_{ps} \cdot \mathbf{n}_{ps} = cos\theta_{ps}$, where $\theta_{ps} = \omega_{ps}t_{ps}$ and ω_{ps} is the rate of rotation in rad/s. The magnetic flux in this situation is $\Phi_{ps} = \int_{S_{ps}}\mathbf{B}_{ps} \cdot \mathbf{n}_{ps}dS = B_{ps}A_{ps}cos(\omega_{ps}t_{ps})$. Consequently the emf in this case, similar to Eq. (23), is

$$\mathcal{E}_{ps} = -\frac{d\Phi_{ps}}{dt_{ps}} = -\frac{d}{dt_{ps}}(B_{ps}A_{ps}cos(\omega_{ps}t_{ps})) = -B_{ps}A_{ps}\frac{d}{dt_{ps}}(cos(\omega_{ps}t_{ps})) = B_{ps}A_{ps}\omega_{ps}sin(\omega_{ps}t_{ps}) \tag{27}$$

and consequently from Ohm's law the induced current is

$$I_{ps} = \left|\frac{\mathcal{E}_{ps}}{R_{ps}}\right| = \frac{B_{ps}A_{ps}\omega_{ps}}{R_{ps}}sin(\omega_{ps}t_{ps}) \tag{28}$$
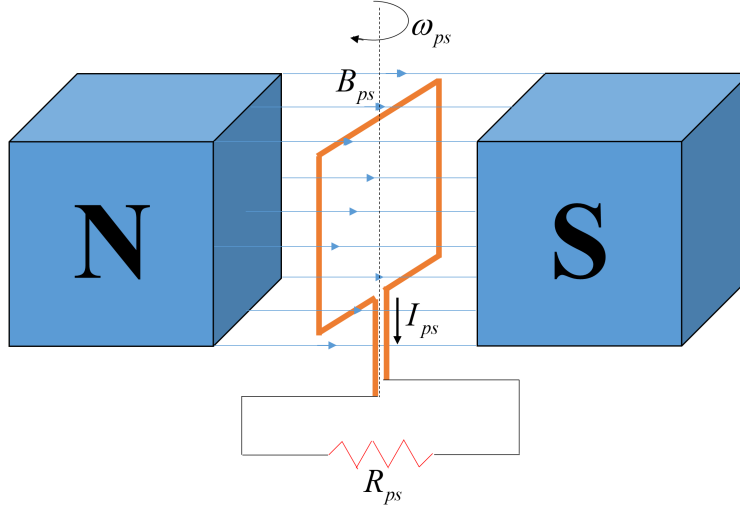
14

Figure 2: A circuit rotating in a magnetic field

where R_{ps} is the resistance provided by the circuit.

Pure dimensional scaling

Consider again the application dimensional analysis where two Pi groups pertinent to this problem are $\Pi_{ps}^1 = \frac{B_{ps} A_{ps} \omega_{ps}}{I_{ps} R_{ps}}$ and $\Pi_{ps}^2 = \omega_{ps} t_{ps}$. Invariance to scale requires that $\Pi_{ps}^1 = \Pi_{ts}^1$ and $\Pi_{ps}^2 = \Pi_{ts}^2$, which provides

$$\Pi_{ts}^1 = \frac{B_{ts} A_{ts} \omega_{ts}}{I_{ts} R_{ts}} = \frac{\beta^2}{g} \frac{B_{ts} A_{ps} \omega_{ps}}{I_{ts} R_{ts}} = \frac{\beta^3}{g} \frac{B_{ts} A_{ps} \omega_{ps}}{I_{ts} R_{ps}} = \frac{\beta^3}{g} \frac{B_{ts}}{B_{ps}} \frac{I_{ps}}{I_{ts}} \Pi_{ps}^1 \tag{29}$$

where use is made of $\omega_{ts} = g^{-1} \omega_{ps}$, which follows from $\Pi_{ps}^2 = \omega_{ts} t_{ts} = g \omega_{ts} t_{ps} = g \frac{\omega_{ts}}{\omega_{ps}} \Pi_{ps}^2$ on setting $\Pi_{ps}^2 = \Pi_{ts}^2$.

The analysis follows that provided above and returns $g = \beta^3$ (or $\omega_{ts} = \beta^{-3} \omega_{ps}$) under the constraints that $B_{ts} = B_{ps}$, $R_{ts} = \beta^{-1} R_{ps}$ and $I_{ts} = I_{ps}$.

Zeroth-order finite similitude

Finite similitude returns the same result on consideration of the relevant zeroth-order field relationships, which are $\mathbf{J}_{ps}^f = \alpha_0^{\rho^f} g \beta^2 \mathbf{J}_{ts}^f$, $\mathbf{B}_{ps} = \alpha_0^M g \beta^2 \mathbf{B}_{ts}$, $\mathbf{E}_{ps} = \alpha_0^F g \beta^2 \mathbf{E}_{ts}$, and the scalar identity $\alpha_0^F = g \beta^{-1} \alpha_0^M$. Ohm's law in field form is $\mathbf{J}^f = \sigma \mathbf{E}$, and the condition $\mathbf{J}_{ps}^f = \beta^2 \mathbf{J}_{ts}^f$ (current matching) provides $\mathbf{E}_{ps} = \beta^2 \mathbf{E}_{ts}$ (with $\sigma_{ts} = \sigma_{ps}$ assumed) and consequently $\alpha_0^F g \beta^2 = \beta^2$, which provides $\alpha_0^F = \beta^2 \alpha_0^M$ (since by assumption $\mathbf{B}_{ps} = \mathbf{B}_{ts}$), but since $\alpha_0^F = g \beta^{-1} \alpha_0^M$ it follows that $g = \beta^3$. This result is in accordance with dimensional analysis providing the relationship $\omega_{ts} = \beta^{-3} \omega_{ps}$ for rotational angular velocities.

Note how to all intents and purposes the analysis with finite similitude is unaffected by the change in problem type. This is a consequence of the field relationships (across the scales) being fixed and rooted to

the fundamentals of electromagnetism (i.e., Maxwell equations). The degrees of freedom available to any analysis is clear from the outset and with scale set (i.e., β fixed) the available freedoms is limited to α_0^F and g only. Although α_0^M appears (and $\alpha_0^{\rho^f}$ above although not needed) in the analysis it is constrained by the relationship $\alpha_0^F = \beta^2 \alpha_0^M$, so is not independent of α_0^F.

4.1.3. Scaling of an RLC circuit

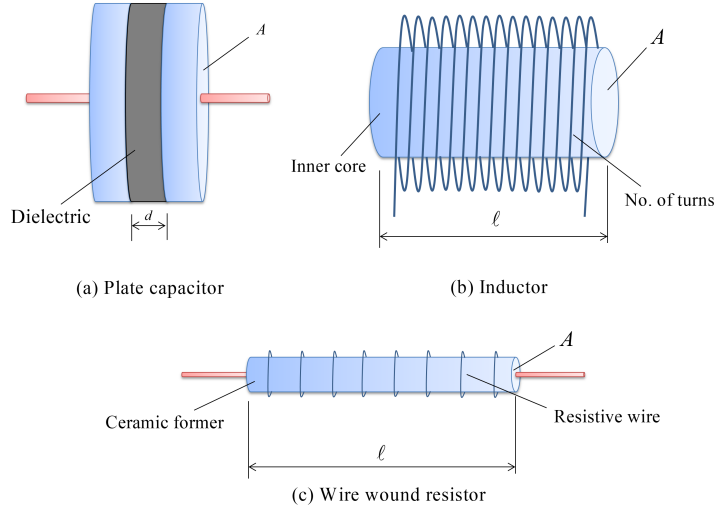(a) Plate capacitor   (b) Inductor

(c) Wire wound resistor

Figure 3: Example designs for RLC circuit components

Depicted in Fig. 3 are typical component designs that might commonly be found in RLC circuits. These types of component are assumed to follow relatively simple standard linear relationships of the form $V_{ps} = I_{ps} R_{ps}$, $V_{ps} = L_{ps} \frac{dI_{ps}}{dt_{ps}}$ and $I_{ps} = C_{ps} \frac{dV_{ps}}{dt_{ps}}$, where V_{ps} is voltage (emf), I_{ps} is current, R_{ps} is resistance, L_{ps} is inductance, and C_{ps} is capacitance. The detailed behaviour of the devices depicted in Fig. 3 satisfy Maxwell equations but it is the circuit response that is the focus of the study in this section. At first sight it might appear that finite similitude is at some disadvantage in this type of analysis when contrasted with dimensional analysis being intimately linked to the fields appearing in Maxwell equations and not voltages and currents. The purpose of this study therefore to demonstrate that circuit type studies under scaling are readily analysed under the finite similitude theory. This is achieved by identifying the particular dominating Maxwell equations that applies to the devices in Fig. 3 and applying the simplifying assumptions invoked to arrive at the standard linear relationships.

The capacitor depicted in Fig. 3 is a device for storing electrical energy by means of the electric displacement field $\mathbf{D}_{ps}$ set up in the dielectric material of permittivity ϵ_{ps}. The electric displacement field is related to charge according to Gauss's relationship Eq. (1a) or equivalently Eq. (10a), which simplifies to $A_{ps} D_{ps} = Q_{ps}^f$, where A_{ps} refers to the surface area in contact with the dielectric for one of the conducting plates, Q_{ps}^f is the free charge at this surface and D_{ts} is the magnitude of the electric displacement field

16

$\mathbf{D}_{ps}$. For the plate capacitor depicted in Fig. 3 it follows that $Q_{ts}^f = A_{ps}D_{ps} = C_{ps}V_{ps}^C$, where the capacitance satisfies the relationship $C_{ps} = \frac{\epsilon_{ps}A_{ps}}{d_{ps}}$ with d_{ps} the separation distance between the conductors, and consequently differentiation of the linear relationship $Q_{ts}^f = C_{ps}V_{ps}^C$ with respect to time t_{ps} provides the sought expression $I_{ps}^f = C_{ps}\frac{dV_{ps}^C}{dt_{ps}}$, where V_{ps}^C is the voltage across the capacitor. An inductor of the type depicted in Fig. 3 is a device for storing magnetic energy by means of the magnetising field $\mathbf{H}_{ps}$ set up in the core of permeability μ_{ps}. The magnetising field is related to current passing through the coil according to Ampere's relationship Eq. (1d) or equivalently Eq. (10d), which simplifies to $H_{ps}\ell_{ps} = I_{ps}^f N_{ps}\ell_{ps}$, where ℓ_{ps} is the length of the core, N_{ps} is the number of turns per unit length, and H_{ps} is the magnitude of the magnetising field $\mathbf{H}_{ps}$. It follows that since $\mathbf{H}_{ps} = \mu_{ps}^{-1}\mathbf{B}_{ps}$ the magnetic field $\mathbf{B}_{ps}$ in the core is of magnitude $B_{ps} = \mu_{ps}I_{ps}^f N_{ps}$. Faraday's law of induction (i.e., $\mathcal{E}_{ps} = -\frac{d\Phi_{ps}}{dt_{ps}}$) for the inductor depicted in Fig. 3 gives the voltage $V_{ps}^L = L_{ps}\frac{dI_{ps}^f}{dt_{ps}}$, where use is made of $\Phi_{ps} = \int_{S_{ps}} \mathbf{B}_{ps} \cdot \mathbf{n}_{ps}dS$ which equals $B_{ps}A_{ps}$ for a single turn of the coil, and where inductance $L_{ps} = \mu_{ps}N_{ps}^2 A_{ps}\ell_{ps}$. The resistor depicted in Fig. 3 is a device that dissipates energy and is assumed to satisfy Ohm's law $V_{ps}^R = I_{ps}^f R_{ps}$, where V_{ps}^R is the voltage across the resistor.

Forming a series RLC circuit from the devices depicted in Fig. 3 means that the sum of the instantaneous voltages V_{ps}^C, V_{ps}^L and V_{ps}^R match the applied voltage V_{ps}^T and consequently the governing differential equation is

$$V_{ps}^T = V_{ps}^L + V_{ps}^R + V_{ps}^C = L_{ps}\frac{dI_{ps}^f}{dt_{ps}} + I_{ps}^f R_{ps} + \frac{Q_{ps}^f}{C_{ps}} = L_{ps}\frac{d^2Q_{ps}^f}{dt_{ps}^2} + R_{ps}\frac{dQ_{ps}^f}{dt_{ps}} + \frac{Q_{ps}^f}{C_{ps}} \tag{30}$$

where use is made of the relationship $I_{ps}^f = \frac{dQ_{ps}^f}{dt_{ps}}$.

The relationships for inductance, capacitance and resistance (i.e., $L_{ps} = \mu_{ps}N_{ps}^2 A_{ps}\ell_{ps}$, $C_{ps} = \frac{\epsilon_{ps}A_{ps}}{d_{ps}}$ and $R_{ps} = \frac{\rho_{ps}\ell_{ps}}{A_{ps}}$) immediately inform on how these quantities change under space scaling on substitution of $\ell_{ts} = \beta\ell_{ps}$, $A_{ts} = \beta^2 A_{ps}$, $N_{ts} = \beta^{-1}N_{ps}$, and under the assumption of replica scaling (i.e., no change in materials) gives $L_{ts} = \beta L_{ps}$, $C_{ts} = \beta C_{ps}$ and $R_{ts} = \beta^{-1}R_{ps}$.

Zeroth-order finite similitude

Since Eq. (30) is concerned with the combination voltages, the expression of particular interest in Table 1 for zeroth order is $V_{ps} = \alpha_0^F g\beta V_{ts}$, which is applicable to each device in the circuit. With the inductor satisfying $V_{ps}^L = L_{ps}\frac{dI_{ps}^f}{dt_{ps}}$ (or $= L_{ps}\frac{d^2Q_{ps}^f}{dt_{ps}^2}$) and since $I_{ps}^f = \alpha_0^{\rho^f} gI_{ts}^f$ (see Table 1) it follows that

$$V_{ps}^L = L_{ps}\frac{dI_{ps}^f}{dt_{ps}} = \alpha_0^{\rho^f} g\beta L_{ps}\frac{dI_{ts}^f}{dt_{ts}} = \alpha_0^F g\beta V_{ts}^L = \alpha_0^F g\beta L_{ts}\frac{dI_{ts}^f}{dt_{ts}} \tag{31}$$

and consequently $\alpha_0^{\rho^f} L_{ps} = \alpha_0^F L_{ts}$ and since replica scaling gives $L_{ts} = \beta L_{ps}$ it follows that $\alpha_0^{\rho^f} = \beta\alpha_0^F$.

Similarly, for the capacitor the voltage and charge relationships $V_{ps}^C = \alpha_0^F g\beta V_{ts}^C$ and $Q_{ps}^f = \alpha_0^{\rho^f} Q_{ts}^f$,

respectively, provide

$$V_{ps}^C = \frac{Q_{ps}^f}{C_{ps}} = \alpha_0^{\rho^f} \frac{Q_{ts}^f}{C_{ps}} = \alpha_0^F g\beta V_{ts}^C = \alpha_0^F g\beta \frac{Q_{ts}^f}{C_{ts}} \tag{32}$$

which leads to $\alpha_0^{\rho^f} C_{ts} = \alpha_0^F g\beta C_{ps}$, but since $C_{ts} = \beta C_{ps}$ for replica scaling it follows that $\alpha_0^{\rho^f} = \alpha_0^F g$ and therefore $g = \beta$.

Consideration of the resistor however poses a problem for replica scaling since $V_{ps}^R = \alpha_0^F g\beta V_{ts}^R$ and $Q_{ps}^f = \alpha_0^{\rho^f} Q_{ts}^f$ from Table 1 provides

$$V_{ps}^R = R_{ps}\frac{dQ_{ps}^f}{dt_{ps}} = \alpha_0^{\rho^f}\beta R_{ps}\frac{dQ_{ts}^f}{dt_{ts}} = \alpha_0^F g\beta V_{ts}^R = \alpha_0^F g\beta R_{ts}\frac{dQ_{ts}^f}{dt_{ts}} \tag{33}$$

which leads to $\alpha_0^{\rho^f} R_{ps} = \alpha_0^F g R_{ts}$ but replica scaling requires $R_{ts} = \beta^{-1}R_{ps}$, which suggests that $\alpha_0^{\rho^f} = \alpha_0^F g\beta^{-1}$ but with $g = \beta$ this condition provides a conflict and confirms that representative behaviour will not be achieved with a single experiment with replica scaling.

The problem can be readily remedied however (for a single scaled experiment) by means of physical modelling where substitution of the condition $\alpha_0^{\rho^f} = \beta\alpha_0^F$ and $g = \beta$ into $\alpha_0^{\rho^f} R_{ps} = \alpha_0^F g R_{ts}$ provides $R_{ps} = R_{ts}$, which is achieved if the resistivity satisfies $\rho_{ts} = \beta\rho_{ps}$. This fix illustrates that for a circuit of such relative simplicity there is little motivation to involve an additional scaled experiment with the application of the first order theory. It is of interest therefore to examine a system of greater complexity that might benefit from an higher order form of finite similitude. Such a system is considered in the next section but note that the satisfaction of the relationship $V_{ps} = \alpha_0^F g\beta V_{ts}$ for each component in the RLC circuit provides,

$$V_{ps}^T = V_{ps}^L + V_{ps}^R + V_{ps}^C = \alpha_0^F g\beta(V_{ts}^L + V_{ts}^R + V_{ts}^C) = \alpha_0^F g\beta V_{ts}^T \tag{34}$$

and consequently the satisfaction of Eq. (30) is replicated perfectly by the trial-space model provided $V_{ps}^T = \alpha_0^F g\beta V_{ts}^T$.

4.2. Induced eddy current in a rod

In order to elevate the complexity of the problem under scrutiny, numerical simulation is applied, where in particular, the Abaqus software [32] is employed here to test the efficacy of the first-order finite similitude theory. The Eddy current problem of interest is suited to a time-harmonic analysis and the Abaqus software makes use of the scalar and vector potentials ϕ and $\mathbf{A}$, where as mentioned above $\mathbf{E} = -\nabla\phi - \frac{\partial\mathbf{A}}{\partial t}$ and $\mathbf{B} = \nabla \times \mathbf{A}$. Note that the first-order similitude identities for ϕ and $\mathbf{A}$ are,

$$\phi_{ps} = \alpha_{01}^F g_1\beta_1\phi_{ts1} + R_1^F(\alpha_{01}^F g_1\beta_1\phi_{ts1} - \alpha_{02}^F g_2\beta_2\phi_{ts2}) \tag{35a}$$

$$\mathbf{A}_{ps} = \alpha_{01}^M g_1\beta_1\mathbf{A}_{ts1} + R_1^M(\alpha_{01}^M g_1\beta_1\mathbf{A}_{ts1} - \alpha_{02}^M g_2\beta_2\mathbf{A}_{ts2}) \tag{35b}$$

which are consistent with $\mathbf{E}$ and $\mathbf{B}$ in Table 1, where as noted above $\alpha_0^F = g\beta^{-1}\alpha_0^M$ and $R_1^F = R_1^M$.

The equation solved in Abaqus is a low frequency approximation of Eq. (1d) (i.e., it neglects displacement current) and takes the form

$$\nabla \times (\mu^{-1} \nabla \times \mathbf{A}_0) + i\omega \sigma^E \cdot \mathbf{A}_0 = \mathbf{J}_0 \tag{36}$$

where ω is natural frequency, $i^2 = -1$, Ohm's law $\mathbf{J}^f = \sigma^E \cdot \mathbf{E}$ is assumed to apply with σ^E being the conductivity tensor, and $\mathbf{A}_0$ and $\mathbf{J}_0$ are the amplitudes of $\mathbf{A}$ and $-\sigma^E \cdot \nabla \phi$, respectively.

(a) Details of the rod-coil assembly

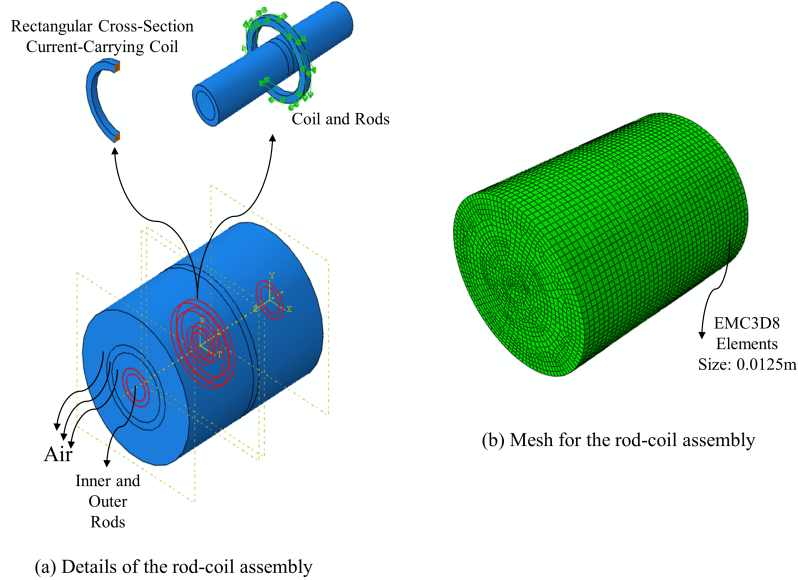(b) Mesh for the rod-coil assembly

Figure 4: A conductive cylindrical rod encircled by a current-carrying coil

The particular problem under scrutiny is presented in Fig. 4 consisting of a conductive cylindrical rod formed from inner and outer components encircled by a rectangular cross-section current-carrying coil. The pertinent dimensions are a radius and length of the full-scale inner rod of $0.035m$ and $0.5m$, respectively. The outer component of the rod of identical length has an outer radius equal to $0.05m$. Additionally, the inner and outer radius, and depth of the encircling conductor is $0.09m$, $0.11m$ and $0.02m$, respectively. The medium surrounding the rod and coil being represented by a cylinder of radius and length of $0.2m$ and $0.5m$ is assumed to have the properties of air. All simulated parts in the assembly are merged to facilitate their representation as a single part of different components. The mesh depicted in Fig. 4 consists of EMC3D8 elements [32] with their sizes given in the figure for the full-scale model. Material properties assigned to the different sections of the full-scale model are tabulated according to Table 2. The properties for the coil and air are considered identical since the current in the coil is directly specified as opposed to modelling the source responsible for the current. The properties of full-scale and small-scale models are listed in Tables 2 and 3. Note that physical modelling is featured here with a simultaneous change of dimensions and materials for the scaled models. The objective here is to demonstrate how the first order theory is capable of representing

Table 2: Electromagnetic properties for coil, air and rod

Model	Air and coil		Rod			
	Conductivity $\Omega^{-1}m^{-1}$	Permeability Hm^{-1} $\times 10^{-7}$	Conductivity $\Omega^{-1}m^{-1}$ $\times 10^{7}$		Permeability Hm^{-1} $\times 10^{-7}$
			Inner	Outer	
Full Scale	1000	4π	6.30 (Silver)	4.11 (Gold)	4π
Trial Model 1	1000	4π	1.03 (Iron)	3.77 (Aluminium)	4π
Trial Model 2	1000	4π	0.699 (Carbon Steel)	5.96 (Copper)	4π

the response of the full-scale model with material properties provided in Table 2. Note additionally that the scaling factors, frequencies and current densities are tabulated in Table 3, where dimensional scaling factors for trial models 1 and 2 are respectively set to be equal to $\beta_1 = 0.50$ and $\beta_2 = 0.25$. This provides a scaling of the dimensions of the full-scale model to half and one quarter of its original size. Trial models 1 and 2 are designed according to the zeroth-order theory, whilst the virtual model being a combination of trial models 1 and 2 is designed according to the first-order theory. In setting the scaling parameters α_0^F and g, two material properties are targeted, which are conductivity σ and permeability μ. Note that permittivity ϵ does not appear in Eq. (36), so there is no reason to target it for this particular problem. The difficulty posed by the problem depicted in Fig. 4 is that it involves a rod in two parts (inner and outer) with different materials and therefore insufficient degrees of freedom for an exact match. Shown above are the constitutive relationships $\mathbf{D}_\beta = \epsilon_\beta \mathbf{E}_\beta$ and $\mathbf{H}_\beta = \mu_\beta^{-1} \mathbf{B}_\beta$, where $\alpha_0^F \epsilon_\beta = \alpha_0^G \epsilon_{ts}$ and $\alpha_0^M \mu_\beta^{-1} = \alpha_0^A \mu_{ts}^{-1}$. Similarly, Ohm's law provides $\mathbf{J}_\beta^f = \sigma_\beta \mathbf{E}_\beta$ where $\alpha_0^F \sigma_\beta = \alpha_0^{\rho^f} \sigma_{ts}$, which is readily confirmed on substitution of the identities $\mathbf{J}_\beta^f = \alpha_0^{\rho^f} g\beta^2 \mathbf{J}_{ts}^f$ and $\mathbf{E}_\beta = \alpha_0^F g\beta^2 \mathbf{E}_{ts}$ (see Table 1). The application of zeroth-order theory to this problem is the identities $\sigma_{\beta_1} = \sigma_{ps}$ and $\mu_{\beta_1}^{-1} = \mu_{ps}^{-1}$ or equivalently $\alpha_{01}^F = \alpha_{01}^{\rho^f} \sigma_{ts1} \sigma_{ps}^{-1}$ and $\alpha_{01}^{\rho^f} g_1 = \alpha_{01}^F \beta_1^2 \mu_{ts1} \mu_{ps}^{-1}$, respectively for the determination of α_{01}^F and g_1, where use is made of the zeroth-order identities $\alpha_{01}^G = g^{-1} \alpha_0^{\rho^f}$, $\alpha_0^A = g\beta^{-1} \alpha_0^G$ and $\alpha_0^F = g\beta^{-1} \alpha_0^M$ to arrive at the expression for g_1. Note that the zeroth-order values in Table 3 make use of the conductivities for the outer rod and consequently results for the inner rod can be expected to suffer the greatest deviation. Taking the zeroth order data forward to first order means that the only unknown is

R_1^F and a first-order improvement on the expression $\alpha_{01}^F \sigma_{ts1}^{-1} = \alpha_{01}^{\rho^f} \sigma_{ps}^{-1}$ is

$$\frac{1}{\sigma_{ps}} = (\frac{\alpha_{01}^F}{\alpha_{01}^{\rho^f}})\frac{1}{\sigma_{ts1}} + R_1^F \left((\frac{\alpha_{01}^F}{\alpha_{01}^{\rho^f}})\frac{1}{\sigma_{ts1}} - (\frac{\alpha_{02}^F}{\alpha_{02}^{\rho^f}})\frac{1}{\sigma_{ts2}} \right) \tag{37}$$

for the determination of R_1^F, which is an expression that can be obtained on dividing through the first-order expression for voltage in Table 1 by $I_{ps}^f \ell_{ps}/A_{ps}$ (since $\sigma_{ps}^{-1} = V_{ps}A_{ps}/(I_{ps}^f \ell_{ps})$) with $A_{ps} = \beta_1^{-2} A_{ts1} = \beta_2^{-2} A_{ts2}$, $\ell_{ps} = \beta_1^{-1}\ell_{ts2} = \beta_2^{-1}\ell_{ts2}$, and under the assumption $I_{ps}^f = \alpha_{01}^{\rho^f} g_1 I_{ts1}^f = \alpha_{02}^{\rho^f} g_2 I_{ts2}^f$. No frequency dependency is assumed for the materials involved, but the frequencies applied satisfy $\omega_{ps} = g_1\omega_{ts1} = g_2\omega_{ts2}$ to ensure frequency matching between projected, virtual and the full scale model. The magnetic field along a

Table 3: The scaling parameters for trial models 1 & 2 and the virtual model

| Model | Scaling parameters | | | | | | Lower and higher frequencies Hz | | Current density A/m^2 $\times 10^7$ | |
	g_1	g_2	$\alpha_0^{\rho^f}$	α_{01}^F	α_{02}^F	R_1^F	First model	Second model	First model	Second model
Full Scale							50		50	
Tri. Mod 1	0.23		1	0.92			218.06		10.96	
Tri. Mod 2		0.09	1		1.45			551.88		110.96
Virtual	0.23	0.09	1	0.92	1.45	0.62	218.06	551.88	10.96	110.96
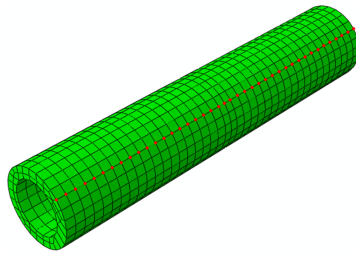
(a) Longitudinal path used for plot
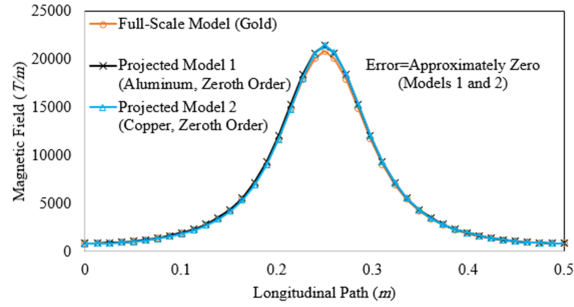
(b) Magnetic field along the outer rod

Figure 5: The magnetic field amplitude measured along a longitudinal path on the outer surface of the outer rod

longitudinal path of the outer rod at full size is predicted using scaled trial models 1 and 2 respectively made from aluminium and copper. The results are presented in Fig. 5, where it is evident that the response of the full-scale outer rod has been captured using the scaled-down trial models with good replication. The successful matching of conductivity and permeability has ensured that there is little error in the magnetic

21
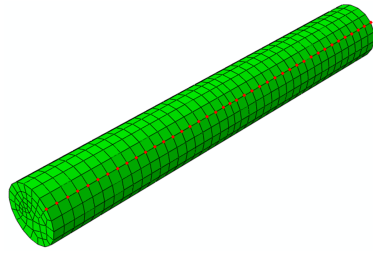
(a) Longitudinal path used for plot
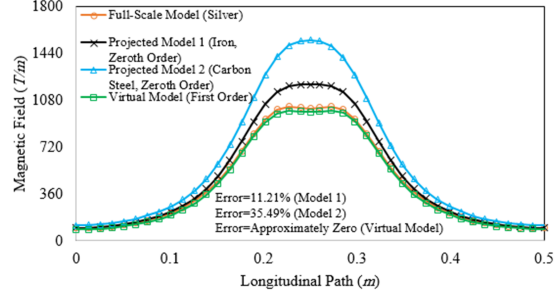
(b) Magnetic field along the inner rod

Figure 6: The magnetic field amplitude measured along a longitudinal path on the outer surface of the inner rod

field prediction for the outer rod. However, examination of Fig. 6, which shows the magnetic field of the full-scale inner rod of silver, is not predicted to a good accuracy using scaled-down trial models 1 and 2, respectively made of iron and carbon steel. The large errors involved in predicting the response behaviour of the full-scale inner rod, which respectively are equal to 11.21% and 35.49% for models 1 and 2, is the result of the zeroth-order theory having insufficient degrees of freedom to capture the pertinent material properties. To deal with this problem, the extra degree of freedom (R_1^F) provided by the first-order theory is used to better match the electrical conductivity of the inner rod. This is achieved by means of Eq. (37) for the determination of R_1^F as tabulated in Table 3 to combine the results of models 1 and 2. The first-order theory provides the magnetic field of the full-scale inner rod along the longitudinal path with approximately zero error.

5. Conclusion

This paper introduces a new scaling theory for electromagnetism, which is able to combine information from more than one scaled experiment. It achieves this by means of new forms of similitude rules, which facilitate the design of scaled experiments with a particular focus here being one and two distinct scales. The approach does not require dimensionless equations and consequently is a step away from the well-known method of dimensional analysis. The following conclusions can be drawn from the work presented in the paper:

- The theory of finite similitude has been further developed to capture all scale dependencies that arise in the field of electromagnetism.

- A transport formulation for Maxwell equations has been established to link the theory of electromagnetism to the finite similitude theory.

22

- By design, the new similitude rules for electromagnetism are nested to ensure that single-experiment rules are contained within two-experiment rules and so on.

- By means of integration, the differential forms of similitude have been shown to capture electromagnetic field behaviours across one and two scaled experiments.

- Scale effects as defined under the well-known theory of dimensional analysis cease to be scale effects under the first-order finite similitude rule, which features proportional field differences.

- The new scaling theory for electromagnetism is shown to be equally applicable to analytical and numerical data.

More specifically, from the simulations performed on the specific electromagnetic systems assesed, it has been shown that:

- Scaled dependencies for inductors, capacitors and resistors have been established and for replica scaling the following relationships, respectively apply: $L_{ts} = \beta L_{ps}$, $C_{ts} = \beta C_{ps}$ and $R_{ts} = \beta^{-1} R_{ps}$.

- Analytical analysis revealed that zeroth-order scaling was able to capture the behaviour of simple systems (e.g., generator, moving rod in a uniform magnetic field) but replica scaling was not possible for the RLC circuit.

- Reproducible behaviour of the RLC circuit by a single experiment was shown to be possible with replica scaling of the inductor and capacitor but the circuit resistance was required to be scale invariant.

- First-order theory proved to be critical in accurately capturing the response of a time-harmonic Eddy current system involving two materials. Errors of some 11.21% and 35.49% obtained with zeroth-order models was reduced to almost 0% with the application of the first-order theory.

References

1. S. Baglio, S. Castorina, N. Savalli, Scaling Issues and Design of MEMS, Wiley, 2008.

2. H. G. Harris, G. M. Sabnis, Structural modeling and experimental techniques, CRC Press, 1999.

3. G. I. Barenblatt, Scaling, Self-Similarity, and Intermediate Asymptotics, Cambridge University Press, 1996.

4. P. W. Bridgman, Dimensional Analysis, Yale University Press, 1922.

5. T. Szirtes, Applied dimensional analysis and modeling, Butterworth-Heinemann, Burlington, MA, 1997.

6. J. H. Brown, G. B. West, Scaling in Biology, Oxford University Press, 2000.

7. J. M. Lirola, E. Castaneda, B. Lauret, M. Khayet, A review on experimental research using scale models for buildings: Application and methodologies, Energy and Buildings 142 (2017) 2–110.

8. K. Casaburo, G. Petrone, F. Franco, S. De Rosa, A review of similitude methods for structural engineering: Application methodologies, Appl. Mech. Rev. 71 (2019) 32.

9. E. Buckingham, On physically similar systems; illustrations of the use of dimensional equations, Phys. Rev. 4 (1914) 345–376. `doi:10.1103/PhysRev.4.345`.
   URL https://link.aps.org/doi/10.1103/PhysRev.4.345

10. A. Varais, X. Roboam, F. Lacressonnière, C. Turpin, J. Cabello, E. Bru, J. Pulido, Scaling of wind energy conversion system for time-accelerated and size-scaled experiments, Mathematics and Computers in Simulation 158 (2019) 65 – 78, eLECTRIMACS 2017, The International Conference on Modeling and Simulation of Electric Machines, Converters and Systems (IMACS TC 1). `doi:https://doi.org/10.1016/j.matcom.2018.05.015`.
    URL http://www.sciencedirect.com/science/article/pii/S0378475418301393

11. L. Cheng, Y. Lin, Z. Hou, M. Tan, J. Huang, W. J. Zhang, Adaptive tracking control of hybrid machines: A closed-chain five-bar mechanism case, IEEE/ASME Transactions on Mechatronics 16 (6) (2011) 1155–1163.

12. A. Jain, T. Nueesch, C. Naegele, P. Lassus, C. Onder, Modeling and control of a hybrid electric vehicle with an electrically assisted turbocharger, IEEE Transactions on Vehicular Technology 65 (6) (2016) 4344–4358, cited By 23. `doi:10.1109/TVT.2016.2533585`.
    URL https://www.scopus.com/inward/record.uri?eid=2-s2.0-84976480750&doi=10.1109%2fTVT.2016.2533585&partnerID=40&md5=242b6dad0b6eb26d1ea51fa7b67b424f

13. W. Li, M. Paul, H. Baig, J. Siviter, A. Montecucco, T. Mallick, A. Knox, A three-point-based electrical model and its application in a photovoltaic thermal hybrid roof-top system with crossed compound parabolic concentrator, Renewable Energy 130 (2019) 400–415, cited By 2. `doi:10.1016/j.renene.2018.06.021`.
URL   https://www.scopus.com/inward/record.uri?eid=2-s2.0-85049342950&doi=10.1016%2fj.renene.2018.06.021&partnerID=40&md5=b52db21dd28b766a5cc1bbeea88f3790

14. M. D. Petersheim, S. N. Brennan, Scaling of hybrid-electric vehicle powertrain components for hardware-in-the-loop simulation, Mechatronics 19 (7) (2009) 1078 – 1090, special Issue on Hardware-in-the-loop simulation. `doi:https://doi.org/10.1016/j.mechatronics.2009.08.001`.
URL http://www.sciencedirect.com/science/article/pii/S0957415809001330

15. M. Ghanekar, D. W. L. Wang, G. R. Heppler, Scaling laws for linear controllers of flexible link manipulators characterized by nondimensional groups, IEEE Transactions on Robotics and Automation 13 (1) (1997) 117–127.

16. K. T. Hsieh, B. K. Kim, One kind of scaling relations on electromechanical systems, IEEE Transactions on Magnetics 33 (1) (1997) 240–244.

17. C. Liu, Y. Bar-Cohen, Scaling laws of microactuators and potential applications of electroactive polymers in MEMS, in: Y. Bar-Cohen (Ed.), Smart Structures and Materials 1999: Electroactive Polymer Actuators and Devices, Vol. 3669, International Society for Optics and Photonics, SPIE, 1999, pp. 345 – 354. `doi:10.1117/12.349692`.
URL https://doi.org/10.1117/12.349692

18. H. Sadeghi, K. Davey, R. Darvizeh, R. Rajabiehfard, A. Darvizeh, An investigation into finite similitude for high-rate loading processes: Advantages in comparison to dimensional analysis and its practical implementation, International Journal of Impact Engineering 140 (2020) 103554. `doi:https://doi.org/10.1016/j.ijimpeng.2020.103554`.
URL http://www.sciencedirect.com/science/article/pii/S0734743X20301354

19. H. Sadeghi, K. Davey, R. Darvizeh, A. Darvizeh, A scaled framework for strain rate sensitive structures subjected to high rate impact loading, International Journal of Impact Engineering 125 (2019) 229 – 245. `doi:https://doi.org/10.1016/j.ijimpeng.2018.11.008`.
URL http://www.sciencedirect.com/science/article/pii/S0734743X18304123

20. H. Sadeghi, K. Davey, R. Darvizeh, A. Darvizeh, Scaled models for failure under impact loading, International Journal of Impact Engineering 129 (2019) 36 – 56. `doi:https://doi.org/10.1016/j.ijimpeng.`

2019.02.010.

URL http://www.sciencedirect.com/science/article/pii/S0734743X18313137

21. M. Moghaddam, R. Darvizeh, K. Davey, A. Darvizeh, Scaling of the powder compaction process, International Journal of Solids and Structures 144-145 (2018) 192 – 212. doi:https://doi.org/10.1016/j.ijsolstr.2018.05.002.
URL http://www.sciencedirect.com/science/article/pii/S0020768318301872

22. R. Ochoa-Cabrero, T. Alonso-Rasgado, K. Davey, Scaling in biomechanical experimentation: a finite similitude approach, Journal of The Royal Society Interface 15 (143) (2018) 20180254. arXiv:https://royalsocietypublishing.org/doi/pdf/10.1098/rsif.2018.0254, doi:10.1098/rsif.2018.0254.
URL https://royalsocietypublishing.org/doi/abs/10.1098/rsif.2018.0254

23. K. Davey, R. Darvizeh, A. Al-Tamimi, Scaled metal forming experiments: A transport equation approach, International Journal of Solids and Structures 125 (2017) 184 – 205. doi:https://doi.org/10.1016/j.ijsolstr.2017.07.006.
URL http://www.sciencedirect.com/science/article/pii/S0020768317303232

24. G. B.Å.S., Scaled analogue experiments in electromagnetic scattering, no. 4 in Light Scattering Reviews, Springer Praxis Books, Berlin, Heidelberg, 2009.

25. G. Sinclair, Theory of models of electromagnetic systems, Proceedings of the IRE 36 (11) (1948) 1364–1370.

26. J. Pries, H. Hofmann, Magnetic and thermal scaling of electric machines, International Journal of Vehicle Design 61 (1-4) (2013) 219–232. arXiv:https://www.inderscienceonline.com/doi/pdf/10.1504/IJVD.2013.050849, doi:10.1504/IJVD.2013.050849.
URL https://www.inderscienceonline.com/doi/abs/10.1504/IJVD.2013.050849

27. R. N. Henriksen, Scale Invariance: Self-Similarity of the Physical World, John Wiley & Sons, Incorporated, 2015.

28. K. Davey, H. Sadeghi, R. Darvizeh, A. Golbaf, A. Darvizeh, A finite similitude approach to scaled impact mechanics, International Journal of Impact Engineering 148 (2021) 103744. doi:https://doi.org/10.1016/j.ijimpeng.2020.103744.
URL https://www.sciencedirect.com/science/article/pii/S0734743X20308149

29. K. Davey, R. Darvizeh, J. Zhang, Finite similitude in fracture mechanics, Engineering Fracture Mechanics 245 (2021) 107573. doi:https://doi.org/10.1016/j.engfracmech.2021.107573.
URL https://www.sciencedirect.com/science/article/pii/S001379442100045X

30. K. Davey, R. Darvizeh, M. Atar, A first order finite similitude approach to scaled aseismic structures, Engineering Structures 231 (2021) 111739. `doi:https://doi.org/10.1016/j.engstruct.2020.111739`. URL https://www.sciencedirect.com/science/article/pii/S0141029620343406

31. A. Sommerfeld, Part iv - maxwell's theory for moving bodies, in: A. Sommerfeld (Ed.), Electrodynamics, Academic Press, 1952, pp. 280–322. `doi:https://doi.org/10.1016/B978-0-12-664662-7.50008-5`. URL https://www.sciencedirect.com/science/article/pii/B9780126646627500085

32. D. S. Simulia, Abaqus 6.14 analysis user's manual, Dassault Systemes (2014).